Obliquely Loaded Welded Attachments Fatigue Categorization in Steel Bridges

Cem Korkmaz and Robert J. Connor

ABSTRACT

The detail category for base metal at the toe of transverse stiffener-to-flange and transverse stiffener-to-web fillet welds is defined as Category C′ in the current AASHTO *LRFD Bridge Design Specifications* (2020, 9th Ed.) and as Category C in the AREMA (2020) *Manual for Railway Engineering* and the AISC *Steel Construction Manual* (2017, 15th Ed.). These are often referred to as short attachments due to their very short length (<51 mm [2 in.]) in the direction of the primary stress range. Sometimes it is necessary to place a stiffener or a connection plate at an angle different than perpendicular to the web, such as in skewed bridges. Increases in the effective length of the stiffener along the flange in the longitudinal direction are seen as the plate is rotated away from being perpendicular to the web. The other extreme occurs when the stiffener is rotated completely 90° and is perfectly parallel to the web and the longitudinal stress range. In this instance, this is identical to the long attachment and classified as Category E (length > 102 mm [4 in.]). The current specifications and manuals, on the other hand, do not have classification on how to address the potential effects on fatigue performance of angles in between these two extremes. This paper summarizes finite element analysis studies based on local stress and structural hot-spot stress approaches that were conducted to investigate and classify welded attachments placed at angles other than 0° (transverse) or 90° (longitudinal) for a variety of stiffener geometries and thicknesses. This study includes new classification for incorporating the findings into the AASHTO *LRFD Bridge Design Specifications*, AREMA *Manual for Railway Engineering*, and the AISC *Steel Construction Manual*.

KEYWORDS: oblique, angular, fatigue categorization, welded attachments, transverse stiffener, local stress, hot spot.

INTRODUCTION

The American Association of State Highway and Transportation Officials' *LRFD Bridge Design Specifications*, 9th Ed. (AASHTO, 2020); the American Railway Engineering and Maintenance-of-Way Association's *Manual for Railway Engineering* (2020); and the American Institute of Steel Construction's *Steel Construction Manual*, 15th Ed. (2017), include a detail category for base metal at the toe of transverse stiffener-to-flange fillet welds and transverse stiffener-to-web fillet welds perpendicular to the web direction. In the AASHTO Specification Table 6.6.1.2.3-1, Condition 7.1, these details are identified as Category C′ (AASHTO, 2020), and the primary stress for this connection detail in the AREMA Manual is Category C in Table 15-1-8, Section 7 (AREMA, 2020), and in the AISC *Manual* Appendix 3, Table A-3.1, Section 7 (AISC, 2017). In skewed steel girder bridges and a variety of other applications, it is occasionally necessary to angle the stiffener or connecting plate away from being perpendicular to the web. As the stiffener is rotated toward the web, thereby increasing the skew angle, the stiffener's effective "length" in the longitudinal direction rises. The most severe instance is when the stiffener is entirely rotated and made parallel to the primary stress range (90°). The detail category for base metal at the weld toe termination of welded attachments more than 102 mm (4 in.) in length and less than 25 mm (1 in.) in thickness is Category E in this situation. Clearly, if the stiffener is entirely rotated to be parallel with the web, it becomes similar to the long attachment, or Category E. These specifications, on the other hand, do not provide guidance on how to handle the potential impacts on fatigue performance of skew angles in between these two extremes.

This paper describes an analytical study focused on classifying the fatigue category for welded attachments placed at angles other than 0° or 90° for a variety of stiffener geometries and thicknesses using local stress and structural hot-spot stress methods. The results are then compared to data obtained through experimental fatigue testing to calibrate the recommendations to actual fatigue performance. Finally, the study includes recommendations for incorporating the findings into the current specifications and manuals.

Cem Korkmaz, PhD, Research Engineer, Lyles School of Civil Engineering, Purdue University, West Lafayette, Ind. Email: ckorkmaz@purdue.edu (corresponding)

Robert J. Connor, PhD, PE, Jack and Kay Hockema Professor, Lyles School of Civil Engineering, Purdue University, West Lafayette, Ind. Email: rconnor@purdue.edu

Paper No. 2021-15

BACKGROUND

It is widely established that the fatigue life of welded attachments is affected by a variety of variables, some of which are difficult to quantify. Fisher et al. (1974) tested more than 150 beams and girders for fatigue strength of transverse stiffeners and attachments under constant amplitude loading to provide the best fit to the test data and limits of dispersion. These and other fatigue test data have confirmed the performance of the typical transverse stiffener as Category C′. Localized stress concentrations, the effect of weld toe defects, residual stresses, and other variables all have an effect on fatigue life. For the attachments discussed in this section, weld toe cracking is the predominant form of cracking. The likelihood of weld toe cracking is uniform regardless of the direction in which the detail is oriented as long as the toe is perpendicular to the applied stress range. In other words, the effects of residual stress and local weld toe defects are virtually identical regardless of the angle when the toe is perpendicular to the applied stress range. However, the local stress concentrations at the weld toe are significantly different as the length of the attachment varies, as evidenced by the reduction in fatigue resistance observed in Figure 1 taken from AASHTO LRFD Table 6.6.1.2.3-1, Condition 7.1 (AASHTO, 2020). As can be seen, the fatigue resistance of the detail reduces from Category C to E solely due to the increase in length. The residual stresses and defect distribution near the weld toe, on the other hand, remain effectively unchanged. Thus, the major element affecting the fatigue resistance of these details as the detail length increases is the stress concentration factor (SCF) near the weld toe.

In his experiments, Quadrato (2010) showed a decrease in fatigue life when the stiffener is obliquely loaded—in other words, when the skew angle was either 30° or 60°. However, there were only four experiments focused on the fatigue category for these welded attachments. Also, it is important to note here that after the Quadrato (2010) experiments, Quadrato et al. (2010) improved new cross-frame connection details for skewed supports as this was the primary focus of that work and was not explicitly focused on fatigue performance of a range of geometries of plate stiffeners. Nevertheless, very useful analytical and experimental data were obtained in that study that were consistent with the results of this more in-depth study on the hot-spot stresses of obliquely oriented stiffeners. Using split pipe bearing stiffeners, Quadrato et al. (2014) also showed an increase both in girder elastic buckling strength and fatigue life.

As indicated, when the welded attachment is rotated 90° and the length parallel to the stress range increases, the SCF also changes (increases) and transitions from the observed fatigue behavior compatible with Category C (or C′) to

Description	Category	Constant A MPa^3 (ksi)	Threshold (ΔF) MPa (ksi)	Potential Crack Initiation Point	Illustrative Examples
Section 7 - Longitudinally Loaded Welded Attachments					
7.1 Base metal in a longitudinally loaded component at a detail with a length L in the direction of the primary stress and a thickness t attached by groove or fillet welds parallel or transverse to the direction of primary stress where the detail incorporates no transition radius				In the primary member at the end of the weld at the weld toe	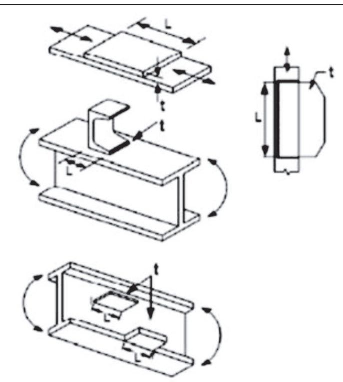
$L < 51$ mm ($L < 2$ in.)	C	144×10^{10} (44×10^{8})	69 (10)		
51 mm ≤ L ≤ 12t *or* 102 mm (2 in. ≤ L ≤ 12t *or* 4 in.)	D	72×10^{10} (22×10^{8})	48 (7)		
L > 12t *or* 102 mm (L > 12t *or* 4 in.)					
$t < 25$ mm ($t < 1.0$ in.)	E	36×10^{10} (11×10^{8})	31 (4.5)		
$t \geq 25$ mm ($t \geq 1.0$ in.)	E'	12.8×10^{10} (3.9×10^{8})	17.9 (2.6)		
(Note: see Condition 7.2 for welded angle or tee section member connections to gusset or connection plates.)					

Fig. 1. Longitudinally loaded welded attachment (AASHTO, 2020).

Table 1. Ratio between the Estimated SCFs from Experimental Data for Detail Categories Normalized to Category C and C′				
Category	Threshold MPa (ksi)	Constant, A MPa^3 (ksi^3)	$A^{1/3}$ MPa (ksi)	Ratio of $A_{C'}^{1/3}/A_x^{1/3}$
C′	83 (12)	144×10^{10} (44×10^{8})	11300 (1640)	1.00
C	69 (10)	144×10^{10} (44×10^{8})	11300 (1640)	Determined according to 49.5-mm (1.95-in.)-long welded attachment
D	48 (7)	72×10^{10} (22×10^{8})	8970 (1300)	1.26
E	31 (4.5)	36×10^{10} (11×10^{8})	7120 (1030)	1.59

Category E. Unfortunately, estimating the SCF at the weld toe given the details of interest is a challenging problem. Fortunately, experimental data exist for both extremities of the skew angle of consideration, namely Category C (or C′) at 0° and Category E at 90°. Given that all other parameters affecting fatigue resistance effectively remain constant (i.e., weld toe defects, residual stresses, etc.), the ratios of the fatigue resistance curves for Categories C (or C′) and E can be used as "anchors" to which the estimated SCF at other angles can be calibrated.

There is some uncertainty whether Category C′ or Category C would be applicable based on the length of the attachment. For instance, a typical stiffener is around 13 mm (½ in.) thick; however, a 32-mm (1¼-in.)-thick bearing stiffener, plus the length added by the fillet welds, is over 50 mm (2 in.) long. It would appear that thicker stiffeners (e.g., bearing stiffeners) should be categorized as Category D; however, AASHTO (2020) makes no such distinction, and all transverse stiffeners are typically classified as C′ regardless of the actual toe-to-toe dimension in the longitudinal direction.

METHODOLOGY

Estimated Stress Concentration Factor Ratios

The purpose of this work was to conduct an analytical study in which the angle of the welded attachment was varied between 0° and 90° to determine the stress concentration factor (SCF). A mesh convergence analysis was conducted to verify that the ratio of estimated SCF ratios for Categories C′ and E remained constant. Again, it is not necessary to know the precise SCF value; rather, it is necessary to be able to anticipate the same ratio of fatigue life as that seen between the two categories that effectively "anchor" the extreme geometries and are based on experimental test results. As seen in Equation 1, the sole variable utilized to describe the difference in fatigue resistance across the various AASHTO details is the detail constant A. Due to the fact that the other parameters determining fatigue life are assumed to remain constant, the ratio of the cube roots of the detail constants is a good measure of the change in the SCF associated with Category C′ and E for a given value of N. In Table 1, this ratio is standardized to Category C′, and x symbolizes different categories (C′, C, D, or E).

$$\frac{(\text{SCF})_x}{(\text{SCF})_{C'}} = \frac{(\Delta F)_{C'}}{(\Delta F)_x} = \left(\frac{A_{C'}/N}{A_x/N}\right)^{1/3} = \frac{(A_{C'})^{1/3}}{(A_x)^{1/3}} \tag{1}$$

While the actual SCF remains unknown, Table 1 indicates that the SCF associated with Category E is approximately 1.6 times that of Category C in the finite life portion of the *S-N* curve. As a result, the ratio of SCFs may be determined. These SCF values are also used in the second stage of the finite element analysis (FEA) to compare to the structural hot-spot stress approach.

Local Stress Finite Element Analysis Approach

The first step in conducting parametric research is to choose the specimen geometry to be examined. While other plate sizes might have been investigated, it was decided to employ components that were equivalent to those used in earlier NCHRP experiments by Fisher et al. (1974). The following plate sizes were modeled in detail:

- Flange width: 406.4 mm (16 in.)
- Flange thickness: 12.7 mm (0.5 in.) [7.2 mm was used in the original NCHRP experimental program (Fisher et al., 1974)]
- Flange length: 508 mm (20 in.)
- Attachment (stiffener) widths: 203.2, 254, and 304.8 mm (8, 10, and 12 in.) (transverse to web at 90°)

- Attachment (stiffener) thickness: 12.7 mm (0.5 in.)
- Weld thickness: 7.9 mm (5⁄16 in.)

The typical configuration is shown in Figure 2. As can be seen in the figure, the attachment was then rotated to evaluate the effect on the estimated SCF. The angles evaluated included 0°, 15°, 30°, 45°, 60°, 75°, and 90°. It is also important to note the stresses were transferred solely through the welds, the attachment plate was not directly tied to the flange.

ABAQUS (2017) was used to generate and evaluate finite element models of the aforementioned geometries. All geometries were exposed to a 6.9 MPa (1 ksi) tensile stress on the gross section area throughout the plate's length. Three-dimensional models were built and subjected to quasi-static implicit analysis using large deformation theory.

A mesh convergence study was conducted with the goal of discovering a mesh with a constant ratio between the various estimated SCF ratios. The SCF ratios for the various meshes for longitudinal stresses on 203.2 mm (8 in.) wide stiffener are presented in Table 2, but in the final study, stiffeners with a width of 203.2, 254, and 304.8 mm (8, 10, and 12 in.) were examined. It should be mentioned

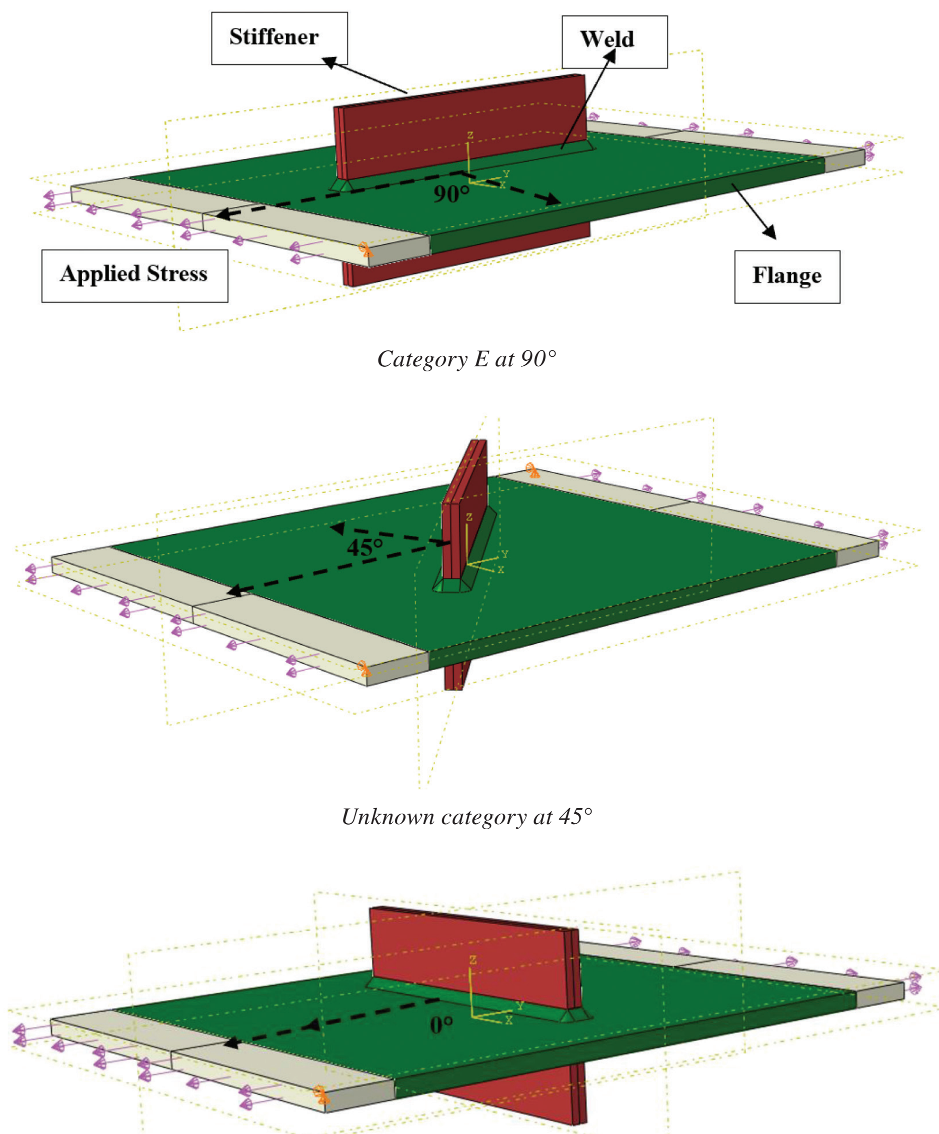

Category E at 90°

Unknown category at 45°

Category C′ at 0°

Fig. 2. Annotated sketches of attachments with different orientations modeled.

Table 2. Estimated SCF for the Various Meshes for Longitudinal Stresses of 200-mm (8-in.)-Wide Stiffener			
Angle (°)	3.81 mm (0.150 in.) Elements SCF Longitudinal Stress Range	3.18 mm (0.125 in.) Elements SCF Longitudinal Stress Range	2.54 mm (0.100 in.) Elements SCF Longitudinal Stress Range
90	2.37	2.65	2.85
75	2.40	2.58	2.80
60	2.38	2.44	2.59
45	1.94	2.12	2.30
30	1.78	1.80	1.98
15	1.67	1.75	1.88
0	1.63	1.72	1.85

Table 3. Ratio between the Estimated SCFs for the Various Meshes for 200-mm (8-in.)-Wide Stiffener—Each Angle Normalized to Category C′ (0°)			
Angle (°)	3.81 mm (0.150 in.) Elements Ratio to C′ (0°)	3.18 mm (0.125 in.) Elements Ratio to C′ (0°)	2.54 mm (0.100 in.) Elements Ratio to C′ (0°)
90	1.46	1.54	1.54
75	1.47	1.50	1.51
60	1.46	1.42	1.40
45	1.19	1.23	1.24
30	1.09	1.05	1.07
15	1.02	1.01	1.01
0	1.00	1.00	1.00

Table 4. Difference between 3.18 mm (0.125 in.) Mesh and 2.54 mm (0.100 in.) Mesh for 200-mm (8-in.)-Wide Stiffener			
Angle (°)	3.18 mm (0.125 in.) Elements Ratio to C′ (0°)	2.54 mm (0.100 in.) Elements Ratio to C′ (0°)	|Difference| (%)
90	1.54	1.54	0.25
75	1.50	1.51	0.77
60	1.42	1.40	1.40
45	1.23	1.24	0.65
30	1.05	1.07	2.01
15	1.01	1.01	0.01
0	1.00	1.00	0.00

that the authors also evaluated the SCF ratios using principal stresses and discovered that the findings were same as obtained when comparing the results using longitudinal stresses as expected.

Further mesh refinement resulted in higher estimations of the actual SCF, as predicted. However, as previously stated, the exact value of the SCF is unimportant. Rather than that, it is the ratio of the different SCF components that is significant. Thus, when the ratio of the SCF (shown in Tables 3 and 4) became virtually constant while the mesh size was changed, the mesh size was considered acceptable.

By examining Tables 3 and 4, it is clear that at a mesh size of 2.54 mm (0.100 in.), the ratio of estimated SCFs becomes virtually constant. With this mesh size, the average difference was 0.65%, while the maximum difference was 2%. As a result, this fine mesh size was determined to be suitable for the purposes of this study.

The mesh details of a typical design are seen in Figure 3. The finite elements used were 20-node quadratic brick elements with reduced integration (C3D20R, per ABAQUS designation). The quadratic formulation is classically utilized in the calculation of large strain gradients, such as the ones occurring at stress risers, in elastic problems.

The maximum longitudinal stresses in the flange were determined using finite element analysis, as seen in Figure 4. Because normal applied stresses were equal to 6.9 MPa (1 ksi), the stress concentration factor was equal to the highest FE longitudinal stress—that is, unlike main SCFs. (It should be mentioned that the authors assessed the ratios in the SCF for primary stresses and discovered that they were identical.)

Structural Hot-Spot Stress Approach

The second step in conducting FE research is to apply the structural hot-spot approach. The local stress approach as defined herein is similar to methods applied by the American Petroleum Institute (API) and American Welding Society (AWS) and is well documented in worldwide publications and readily available from Hobbacher at the International Institute of Welding (IIW) (Hobbacher, 2016). It is used extensively for the fatigue evaluation of tubular structures and plate-type structures with complex geometries by various industries, where there is no clearly defined nominal stress due to complicated geometric effects. The local stress approach recognizes that fatigue damage is caused by stress raisers that exist at details and attempts to quantify them by more refined analysis rather than classification.

This approach is based on assessment of the surface stress precisely at the weld toe of the joint. The baseline *S-N* curve is associated with butt weld or fillet weld details in a nominal stress field. In this method, the stress concentration factor accounts for effects associated with global geometry, and any local discontinuities and flaws are incorporated into the *S-N* curve. The reader is invited to review Niemi et. al (2018) for more information.

The same finite element models were used. In the hot-spot determination, the paths were drawn to obtain the base plate surface stresses. In Figure 5, the path lines were drawn from the maximum longitudinal stress location at the weld toe in the direction of stresses.

Because of the oblique orientation of the stiffeners, it is hard to use uniform meshes. According to Niemi et al. (2018) and Hobbacher (2016), when a nonuniform mesh is used, relatively fine meshes that are smaller than 0.4 times the thickness of the base plate should be preferred. The mesh sizes that are 3.18 mm (0.125 in.) and 2.54 mm (0.100 in.) utilized in this area are less than 0.4 times the thickness 5.08 mm (0.2 in.). Because there is no misalignment, the stress state is almost uniaxial, and the structural hot-spot stress can be estimated by extrapolating surface stress to the weld toe. Due to this nonuniformity and the complexity of the detail, the fine meshed models were preferred to be used to avoid mesh irregularities. The use of solid element modeling also enables explicit modeling of

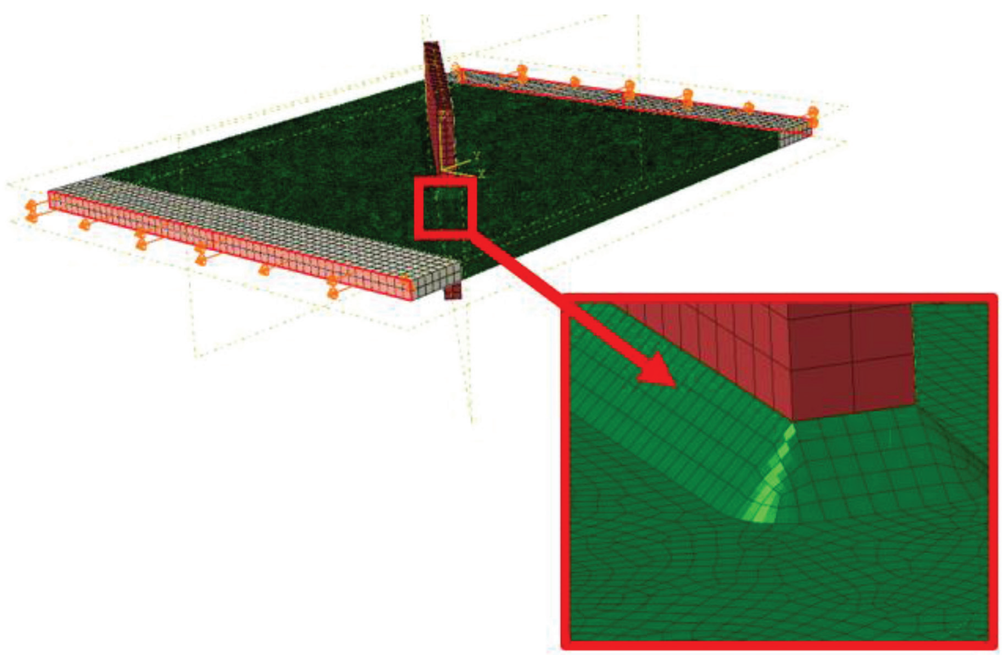

Fig. 3. Solid model (C3D20R) of the specimens.

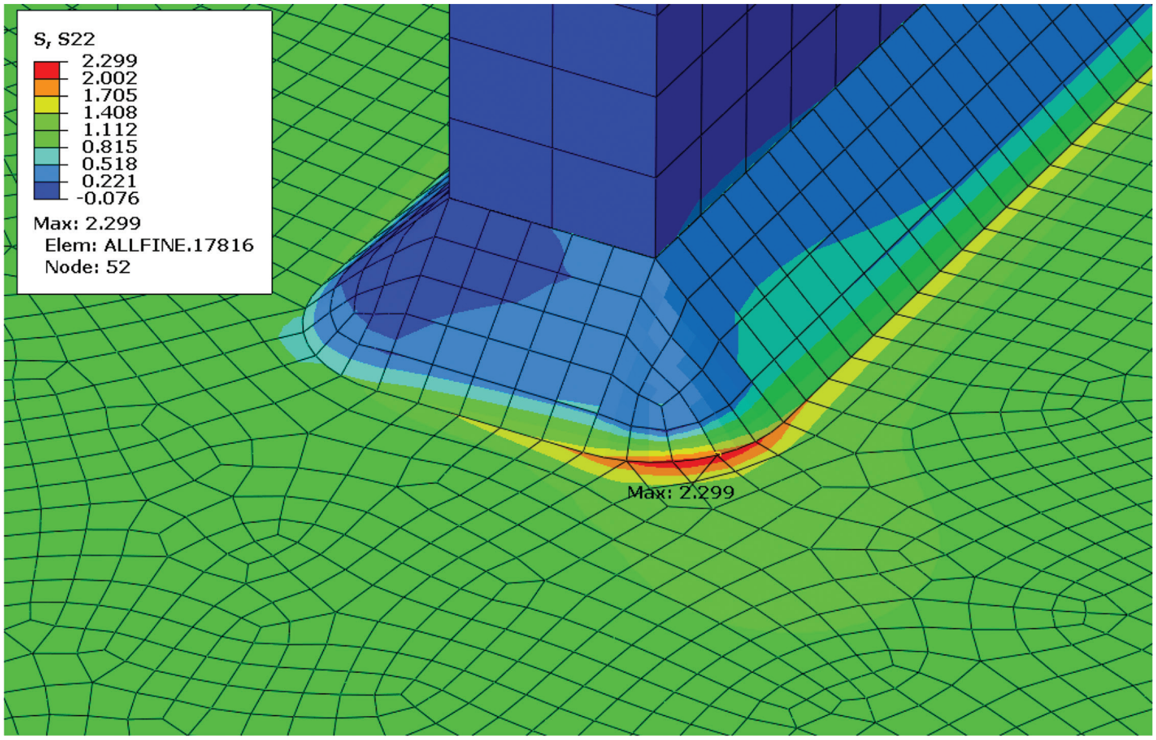

Fig. 4. Example of a solid model maximum longitudinal stresses (ksi) of the specimens.

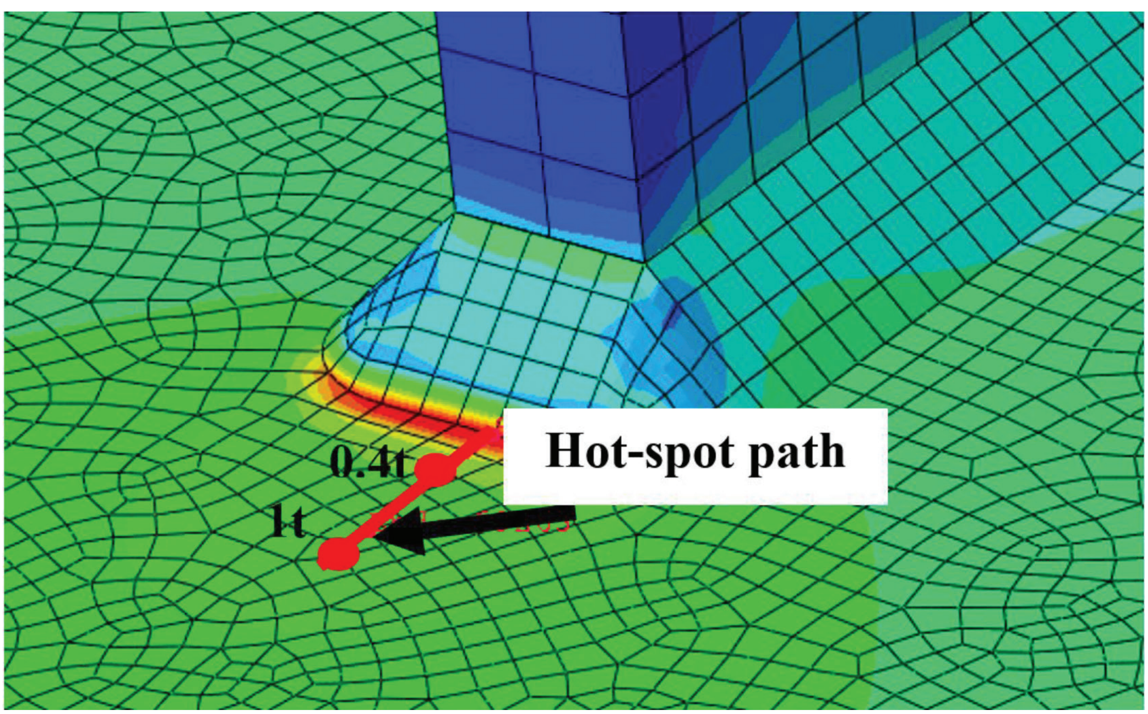

Fig. 5. Solid model maximum longitudinal stresses of the specimens.

Table 5. Structural Hot-Spot Stress Ratio between the Assessed and the Reference Detail

Angle (°)	Hot-Spot Stress Ratio, $\sigma_{hs,assess}/\sigma_{hs,ref}$ for 3.18 mm (0.125 in.) Mesh Size	Hot-Spot Stress Ratio, $\sigma_{hs,assess}/\sigma_{hs,ref}$ for 2.54 mm (0.100 in.) Mesh Size
90	1.52	1.51
75	1.49	1.48
60	1.40	1.41
45	1.24	1.24
30	1.08	1.08
15	1.02	1.02
0	1.00	1.00

the weld geometry. When solid elements are used, Niemi et al. explain that when applied to Type "a" hotspots (only membrane stress), as seen in Equation 2, the linear extrapolation technique must make use of nodal stresses of 0.4 and 1.0 times of the base metal thickness, t, at the weld toe:

$$\sigma_{hotspot} = 1.67x\sigma_{0.4t} - 0.67x\sigma_{1t} \tag{2}$$

Similar to the localized stress approach discussed earlier, the ratio between the structural hot-spot of the detail to be assessed, $\sigma_{hs,assess}$, and the structural hot-spot of the reference detail, $\sigma_{hs,ref}$, which is defined as Category C′, is important. As expected, further mesh refinement resulted in better estimations of these ratios. Two different fine mesh sizes are compared in Table 5 [3.18 mm (0.125 in.) and 2.54 mm (0.1 in.)]. It is seen that the ratios became virtually constant while the relatively fine mesh size was used.

By examining Table 5, it is clear that at a mesh size of 2.54 mm (0.1 in.), estimated results become virtually constant. With this mesh size, the maximum difference was less than 1%. As a result, this mesh size was determined to be suitable for the purposes of this study.

RESULTS

As stated before, the current study's goal is to estimate an appropriate AASHTO (2020) fatigue category for obliquely loaded welded attachments by comparing the ratio of estimated SCFs and hot-spot stresses to the value associated with Category C′ (90° perpendicular to the applied stresses). Other factors, such as residual stresses caused by weld defects, do not need to be explicitly considered because they are effectively constant regardless of the attachment angle. Additionally, it is known that there may be certain effects at welds that wrap around the stiffener as well as other small geometric effects not included in this research. These effects were deemed negligible, however, because they are not explicitly considered in existing fatigue design or evaluation methodologies. Thus, the load-induced fatigue performance of these details can be estimated by comparing the calculated SCF calibration factor to the known fatigue resistance of welded stiffener connections transverse to the primary stress direction (Category C′) and longitudinally loaded welded attachments (Category E). The following variables are calculated for each geometry analyzed:

- *Longitudinal stress range,* σ_L*:* Total longitudinal force divided by the cross-sectional area of the plate. For all models, this equals the applied traction of 6.9 MPa (1 ksi).
- *Estimated stress concentration factor (SCF):* Stress concentration factors are defined as the maximum longitudinal stresses, σ_L, adjacent to the weld toe divided by remotely applied longitudinal (nominal) stress.
- *SCF calibration factor:* The factor used to scale the fatigue resistance of any attachment oriented between 0° (Category C′) and 90° (Category E) (shown in Equation 3):

$$\text{SCF calibration factor} = 1 + \frac{\text{SCF}_{Angle} - SCF_{0(Category\ C')}}{\text{SCF}_{90(Category\ E)} - \text{SCF}_{0(Category\ C')}} \times 0.59 \tag{3}$$

The same approach was utilized to calibrate the factor for used with the structural hot-spot approach.

- *Principal,* σ_P *stress ranges:* Stress concentration factors and ratios are also obtained for the stress ranges of σ_P that are obtained from the FEA models for comparison purposes.

Due to the fact that the other parameters determining fatigue life remain constant, the ratio of the cube roots of

Table 6. Estimated SCF Values for Various Angles and Stiffener Lengths Based on FEA						
Angle (°)	200 mm (8-in.)-Wide Stiffener Longitudinal Stresses	200 mm (8-in.)-Wide Stiffener Principal Stresses	254 mm (10-in.)-Wide Stiffener Longitudinal Stresses	254 mm (10-in.)-Wide Stiffener Principal Stresses	305 mm (12-in.)-Wide Stiffener Longitudinal Stresses	305 mm (12-in.)-Wide Stiffener Principal Stresses
90	2.85	3.19	2.90	3.30	2.92	3.30
75	2.80	3.04	2.86	3.18	2.87	3.18
60	2.59	2.82	2.66	2.95	2.66	3.00
45	2.3	2.50	2.31	2.58	2.34	2.60
30	1.98	2.14	1.99	2.19	2.00	2.20
15	1.88	2.03	1.88	2.06	1.89	2.08
0	1.85	2.03	1.87	2.05	1.88	2.06

the detail constants is a reasonable indicator of the change in the SCF associated with Categories C and E for a given value of N. In Table 1, SCF is standardized to Category C (C′). Figure 6 presents (1) the factors based on AASHTO lower bound curves (shown as the horizontal dashed lines) and (2) the calibration factor of the estimated SCF from the FEA study normalized to the Category C′ and E. The dashed horizontal lines effectively represent lower bound fatigue resistance in AASHTO that are based on experimental data. The solid curved line represents the calibration factor of the SCF ratios from local stress approach, and the dashed curved line represents the factor of hot-spot stress approach obtained from the FEA when the stiffener angle was changed. Where the dashed lines intersect with the curves, a reasonable estimate of the angle at which fatigue resistance falls into the next *lower* category is obtained. In other words, any values that lie below the dashed Category E line but above the dashed Category D line are best categorized as Category E. The same is true for Categories C/C′ and D.

As stated, Table 6 was generated through FEA and presents the predicted results [as reference to a nominal stress of 6.9 MPa (1 ksi)] for various angles; stiffener lengths of 200, 254, and 305 mm (8, 10, and 12 in.); and stresses (i.e., longitudinal, and principal). Comparing the SCF ratios in Table 6 for a given angle but for different stiffener lengths

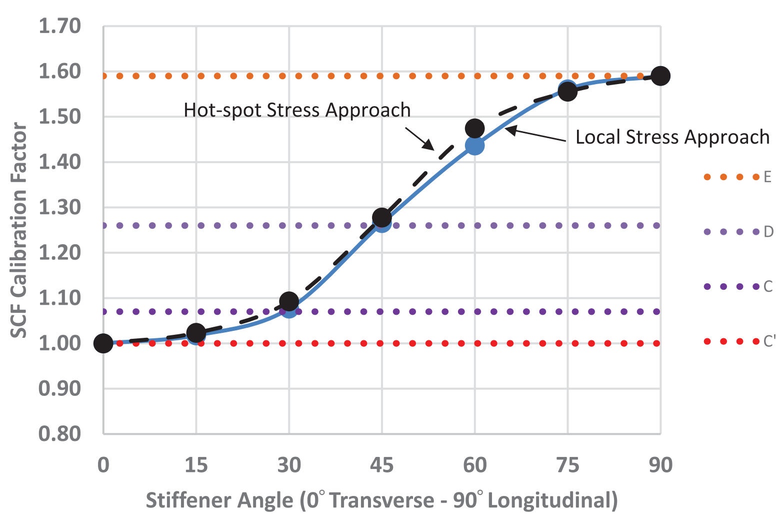

Fig. 6. SCF calibration factor of the estimated SCF and hot-spot stresses from the FEA study vs. AASHTO lower-bound fatigue curves.

Table 7. Ratio Estimated SCF Values for Various Angles Based on FEA Normalized to 0°						
Angle (°)	**200 mm (8-in.)-Wide Stiffener Longitudinal Stresses**	**200 mm (8-in.)-Wide Stiffener Principal Stresses**	**254 mm (10-in.)-Wide Stiffener Longitudinal Stresses**	**254 mm (10-in.)-Wide Stiffener Principal Stresses**	**305 mm (12-in.)-Wide Stiffener Longitudinal Stresses**	**305 mm (12-in.)-Wide Stiffener Principal Stresses**
90	1.54	1.57	1.55	1.61	1.56	1.61
75	1.50	1.50	1.53	1.56	1.53	1.55
60	1.42	1.39	1.43	1.44	1.42	1.46
45	1.23	1.24	1.24	1.26	1.25	1.26
30	1.05	1.06	1.06	1.07	1.06	1.07
15	1.01	1.00	1.01	1.01	1.01	1.01
0	1.00	1.00	1.00	1.00	1.00	1.00

shows that the length of the attachment (for the lengths considered) has no appreciable influence as expected. This observation is consistent with the experimental work by Fisher et al. (1974) in which attachments greater than 4 in. were characterized by Category E. Since stiffeners and connections plates will almost always be at least 102 mm (4 in.) or longer, the results apply to the vast majority of cases.

The range of predicted SCF ratios for the various angles and stiffener widths evaluated are shown in Table 7. (These data are also plotted in Figure 6 for SCF ratios based on longitudinal stresses.) The angle of a typical transverse stiffener is standardized to 0° (i.e., the stiffener is perpendicular to the web). As can be seen, at about 45°, the ratio in the SCF is nearly 1.26 when longitudinal stresses are considered (i.e., 1.232) and almost exactly 1.26 for when principal or von Mises stresses are considered. As a result, when the stiffener is at 45°, it is determined that Category D should offer a reasonable estimate of the fatigue life. Additionally, good agreement is seen when data for Category E are included.

As shown in Figure 6, the data indicate that once the stiffener is angled more than about 20° to 25°, the SCF increases above that associated with Category C′. This indicates that Category C′ may be unconservative and the fatigue resistance should be estimated with the next unique lower category (i.e., Category D). Clearly, many bridges would be affected by a reduction to Category D due to the sheer number of bridges built that are slightly skewed (i.e., just below 90°). In order to reduce the impact and a significant drop in fatigue resistance (i.e., from C′ to D), incorporating Category C for this range of angles was studied as will be discussed later.

Based on the AASHTO fatigue illustrations, Category C is applicable to “short” attachments that are 50 mm (2 in.) or less in length. While Category C and C′ share the same finite life characteristics, the constant-amplitude fatigue threshold (CAFL) for Category C′ is slightly higher. This is because Category C′ details are generally shorter than 50 mm (2 in.) and possess a slightly lower SCF. Note, the residual stresses and defect distribution at the weld toe would be expected to be the same for both C and C′. Thus, while the finite life portion can be estimated easily, the authors attempted to identify the angle at which the SCF of a stiffener (i.e., C′) equals that associated with C. This was done by comparing the estimated SCF ratios as the length of the attachment approached up to 50 mm (2.0 in.) in length. Figure 7 illustrates the model used to obtain this estimated SCF.

Table 8 presents the estimated SCF for two transverse stiffeners or attachments of different thickness attached to the flange with only fillet welds. While the SCF for the 13 mm (0.5-in.)-thick stiffener corresponds to Category C′, the 49.5 mm (1.95-in.)-thick stiffener corresponds to Category C. In other words, the SCF of 1.981 for the 1.95-in.-long attachment effectively represents that associated with Category C [i.e., a detail that is almost 50 mm (2 in.) long and hence at the limit of Category C]. By taking the ratio of these two SCFs and plotting the value on Figure 6, the angle at which Category C can be applied can be estimated. As can be seen, this angle corresponds to about 30°. It is also apparent from the data in Table 7 and as plotted in Figure 6, that between 0° and about 15°, there is only about a 1.5% change in the ratio when normalized to the SCF of Category C′. Hence, there is really no need to drop below

Table 8. Comparison of SCF Obtained from FEA for 12.7 and 49.5 mm-Thick Attachments		
Angle (°)	**12.7 mm (0.5-in.)-Thick SCF**	**49.5 mm (1.95-in.)-Thick SCF**
0	1.85	1.98

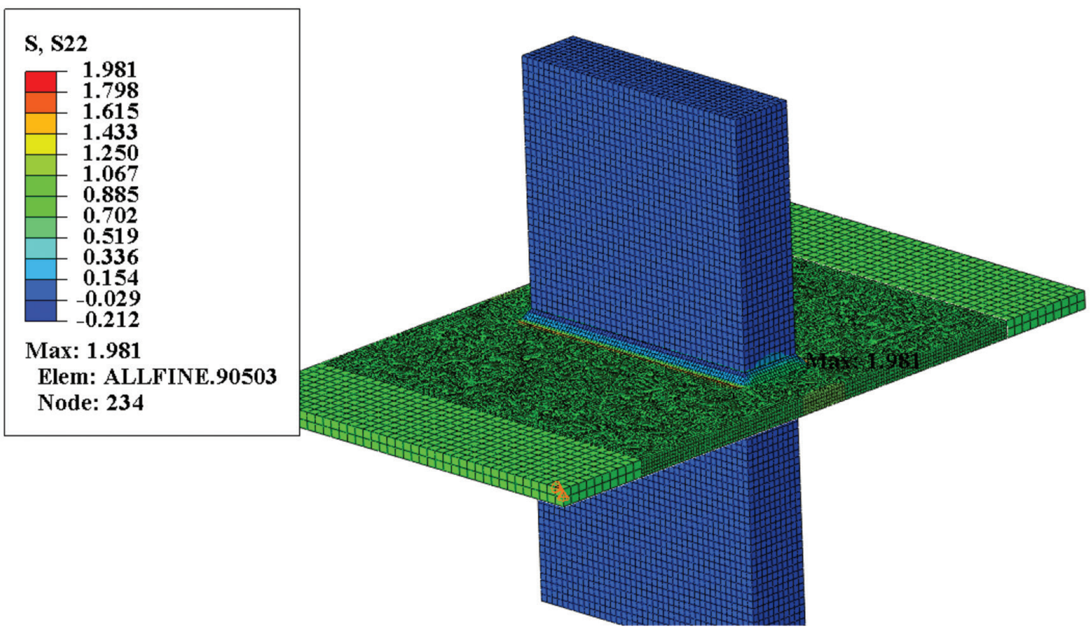

Fig. 7. FE model of 49.5 mm (1.95-in.)-thick stiffener to estimated SCF for Category C.

Category C′ for stiffeners angled between 0° and 15° and C can then be applied between 15° and 30°. Above 30° would thus apply.

$$\text{Category C (SCF)} = \frac{1.98}{1.85} = 1.07$$

It is also apparent that once the angle exceeds 45°, the increase in the SCF indicates that Category E is more applicable.

The final recommendations are summarized in Figure 8, where the proposed category versus skew angle is presented. It is noted that Figure 8 and throughout this study, the references to the skew angle are opposite from that typically used in AASHTO.

CONCLUSIONS

All stiffeners in the current research were 12.7 mm (0.5 in.) thick because this thickness is commonly utilized in steel bridge girders. Additionally, it is equivalent to the stiffener thickness used in the NCHRP experiments (Fisher et al., 1974) [7.2 mm (9⁄32 in.)]. Additionally, the stiffener's length was changed between 200, 254, and 305 mm (8, 10, and 12 in.). Additional FEA, and possibly experimental data,

Description	Category	Constant *A* MPa^3 (ksi^3)	Threshold $(\Delta F)_{TH}$ MPa (ksi)	Potential Crack Initiation Point	Illustrative Examples
Base metal in a longitudinally loaded component at an obliquely oriented detail with an effective length *L* > 102 mm (4 in.) and a thickness *t* less than 25 mm (1 in.) attached by groove or fillet welds.				In the primary member at the weld toe	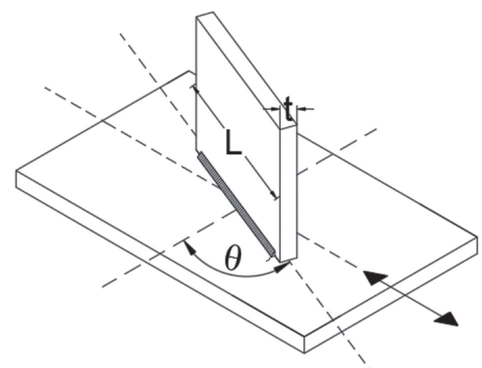
θ ≤ 15°	C'	144 x 10^{10} (44 x 10^8)	83 (12)		
15° < θ ≤ 30°	C	144 x 10^{10} (44 x 10^8)	69 (10)		
30° < θ ≤ 45°	D	72 x 10^{10} (22 x 10^8)	48 (7)		
45° < θ ≤ 90°	E	36 x 10^{10} (11 x 10^8)	31 (4.5)		

Fig. 8. Recommended provisions for skewed plates based on the skew angle.

may be required for thicker stiffeners and associated angles of orientation. One possibility is to simply increase the recommendations for thicker stiffeners when they are used, but the authors feel this would require more research. Based on the results of the current study, it is noted that the transition between Categories C and C′ was best represented at an angle of 15°. The limit for Category D is 45°. Beyond 45°, it is recommended that higher angles are classified as Category E.

REFERENCES

AASHTO (2020), *LRFD Bridge Design Specifications (customary U.S. units)*, 9th Ed., American Association of State Highway and Transportation Officials, Washington, D.C.

ABAQUS (2017), Simulia, Dassault Systems, Boston, Mass.

AREMA (2020), *Manual for Railway Engineering*, American Railway Engineering and Maintenance-of-Way Association, Lanham, Md.

AISC (2017), *Steel Construction Manual*, 15th Ed., American Institute of Steel Construction, Chicago, Ill.

Fisher, J.W., Pedro, A.A., Yen, B.T., Klingerman, D.J., and Mcnamee, B.M. (1974), "Fatigue Strength of Steel Beams with Welded Stiffeners and Attachments," NCHRP Synthesis 147, National Academy Press, Washington, D.C.

Hobbacher, A.F. (2016), "Recommendations for Fatigue Design of Welded Joints and Components," *IIW Collections*, https://doi.org/10.1007/978-3-319-23757-2_7.

Niemi, E., Fricke, W., and Maddox, S.J. (2018), *Structural Hot-Spot Stress Approach to Fatigue Analysis of Welded Components Designer's Guide*, Springer Singapore, Singapore.

Quadrato, C. (2010), "Stability of Skewed I-Shaped Girder Bridges Using Bent Plate 227 Connections," PhD Dissertation, University of Texas, Austin, Texas.

Quadrato, C., Battistini, A., Frank, K., Helwig, T., and Engelhardt, M. (2010), "Improved Cross-Frame Connection Details for Steel Bridges with Skewed Supports," *Transportation Research Record: Journal of the Transportation Research Board*, Vol. 2200, No. 1, pp. 29–35.

Quadrato, C., Battistini, A., Helwig, T., Engelhardt, M., and Frank, K. (2014), "Increasing Girder Elastic Buckling Strength Using Split Pipe Bearing Stiffeners," *Journal of Bridge Engineering*, Vol. 19, No. 4, 04013017.